High-resolution observations of IRAS 08544-4431

Detection of a disk orbiting a post-AGB star and of a slow disk wind

V. Bujarrabal¹, A. Castro-Carrizo², H. Van Winckel³, J. Alcolea⁴, C. Sánchez Contreras⁵, M. Santander-García^{4,6}, and M. Hillen³

- Observatorio Astronómico Nacional (OAN-IGN), Apartado 112, E-28803 Alcalá de Henares, Spain e-mail: v.bujarrabal@oan.es
- ² Institut de Radioastronomie Millimétrique, 300 rue de la Piscine, 38406, Saint Martin d'Hères, France
- ³ Instituut voor Sterrenkunde, K.U.Leuven, Celestijnenlaan 200B, 3001 Leuven, Belgium
- ⁴ Observatorio Astronómico Nacional (OAN-IGN), C/ Alfonso XII, 3, E-28014 Madrid, Spain
- ⁵ Centro de Astrobiología (CSIC-INTA), Ctra. M-108, km. 4, E-28850 Torrejón de Ardoz, Madrid, Spain
- 6 Instituto de Ciencia de Materiales de Madrid (CSIC). Calle Sor Juana Inés de la Cruz 3, E-28049 Cantoblanco, Madrid, Spain

Received 5 December 2017 / Accepted 23 January 2018

ABSTRACT

Aims. In order to study the effects of rotating disks in the post-asymptotic giant branch (post-AGB) evolution, we observe a class of binary post-AGB stars that seem to be systematically surrounded by equatorial disks and slow outflows. Although the rotating dynamics had only been well identified in three cases, the study of such structures is thought to be fundamental to the understanding of the formation of disks in various phases of the late evolution of binary stars and the ejection of planetary nebulae from evolved stars.

Methods. We present ALMA maps of 12 CO and 13 CO J=3–2 lines in the source IRAS 08544–4431, which belongs to the above mentioned class of objects. We analyzed the data by means of nebula models, which account for the expectedly composite source and can reproduce the data. From our modeling, we estimated the main nebula parameters, including the structure and dynamics and the density and temperature distributions. We discuss the uncertainties of the derived values and, in particular, their dependence on the distance

Results. Our observations reveal the presence of an equatorial disk in rotation; a low-velocity outflow is also found, probably formed of gas expelled from the disk. The main characteristics of our observations and modeling of IRAS 08544–4431 are similar to those of better studied objects, confirming our interpretation. The disk rotation indicates a total central mass of about 1.8 M_{\odot} , for a distance of 1100 pc. The disk is found to be relatively extended and has a typical diameter of $\sim 4~10^{16}$ cm. The total nebular mass is $\sim 2~10^{-2}$ M_{\odot} , of which $\sim 90\%$ corresponds to the disk. Assuming that the outflow is due to mass loss from the disk, we derive a disk lifetime of ~ 10000 yr. The disk angular momentum is found to be comparable to that of the binary system at present. Assuming that the disk angular momentum was transferred from the binary system, as expected, the high values of the disk angular momentum in this and other similar disks suggest that the size of the stellar orbits has significantly decreased as a consequence of disk formation.

Key words. stars: AGB and post-AGB – circumstellar matter – radio-lines: stars – planetary nebulae: individual: IRAS 08544–4431

1. Introduction

Planetary and preplanetary nebulae (PNe, pPNe) often show a remarkable axial symmetry and fast bipolar outflows with velocities around 100 km s⁻¹. On the contrary, asymptotic giant branch (AGB) circumstellar envelopes, their immediate precursors, are spherical, at least at large-scale, and expand isotropically at moderate velocities $(10 - 20 \text{ km s}^{-1})$. The development of such axial structure and dynamics remains an open question. It has been proposed to be associated with rotating disks (e.g., Soker 2001, Bujarrabal et al. 2001, Balick & Franck 2002, Sánchez Contreras et al. 2002), from which material would fall onto the star or a companion during early post-AGB phases, powering very fast and collimated stellar jets. In principle, the material ejected during the AGB phases does not have enough angular momentum to form Keplerian disks, which should only appear around binary stellar systems, as these systems have the necessary angular momentum stored in their orbital movement. Other mechanisms to explain bipolar post-AGB nebula involve an anisotropic sudden ejection of stellar gas by a very late AGB (or very early post-AGB) star during a common-envelope phase (Alcolea et al. 2007, De Marco et al. 2009, 2011, Iaconi et al. 2017). However, our theoretical understanding of these phenomena is still poor.

The detailed observation of Keplerian disks around post-AGB stars, including their dynamics, is not straightforward, since it requires high angular and spectral resolutions. To date, disks have been well mapped only in three objects, the Red Rectangle, AC Her, and IW Car, by means of interferometric mm-wave maps of CO lines (Bujarrabal et al. 2013b, 2015, 2017). These sources belong to a class of binary post-AGB stars surrounded by low-mass nebulae that show independent evidence of the presence of disks (e.g., Van Winckel 2003, de Ruyter et al. 2006, Gezer et al. 2015, Hillen et al. 2016, 2017). Notably, they are characterized by spectral energy distributions (SEDs) with a significant near-infrared (NIR) excess, revealing the existence hot dust close to the stellar system. The very compact nature of the NIR emission has been confirmed by interferometric IR measurements (e.g., Hillen et al. 2017). In addition, the IR spectra reveal the presence of highly processed grains, which is indicative of the longevity of the disks.

Single-dish observations of ¹²CO and ¹³CO emission in these NIR-excess post-AGB stars (including the Red Rectangle, AC Her, and IW Car) systematically yielded characteristic line profiles, which are exactly those expected from relatively extended Keplerian disks (Bujarrabal et al. 2013a, Bujarrabal & Alcolea 2013). A slowly expanding component was also proposed in most nebulae, although its shape and dynamics could not be well identified from those data. Indeed, ALMA maps of CO lines in the Red Rectangle and IW Car show a bipolar lowvelocity outflow, which is particularly noticeable in lines with relatively high opacity and excitation; this bipolar outflow was deduced to be very probably formed of gas extracted from the disk, given its structure and kinematics. The CO emission image of 89 Her, another NIR-excess post-AGB, is dominated by an extended hourglass-like nebula in slow expansion (Bujarrabal et al. 2007). Although rotation was not actually resolved in 89 Her, a small disk could be confined to the prominent central clump. Recent NOEMA maps of the similar objects IRAS 19125+0343 and R Sct (Gómez-Garrido et al., in preparation) also show an expanding nebula and a possible central disk that remains unresolved. On the other hand, no gas in expansion was found in the mm-wave maps of AC Her, but we cannot rule out a diffuse outflow, since the CO interferometric data show a significant flux loss and no sub-mm observations exist.

We stress that no signs of Keplerian disks have been found in other kinds of post-AGB nebulae, in particular in the wellobserved high-mass pPNe and young PNe. We cannot exclude that confusion with the strong emission from their expanding nebulae prevents in some way the detection of emission from small central disks, but even high-resolution observations of the very inner nebular regions have yielded no sign of disks to date (e.g., Alcolea et al. 2007, Olofsson et al. 2015, Santander-García et al. 2017). The presence of binary systems in the center of high-mass bipolar pPNe and PNe is also debated. Some well-known nebulae, such as OH231.8+4.2, M2-9, and several evolved PNe, harbor binary systems (see, e.g., Sánchez Contreras et al. 2004, Castro-Carrizo et al. 2012, Hillwig et al. 2016). However, long-term radial velocity studies have yielded negative results in a number of post-AGB sources; for example, Hrivnak et al. (2017) have only found that one object, out of seven well-studied sources, was probably a wide stellar system. These findings imply that there are significant constraints to eventual binarity in these sources.

The evolution of NIR-excess post-AGB objects is not well known (e.g., Van Winckel et al. 2009, De Marco 2014) and could be significantly different from that of well-studied (pre)planetary nebulae. Their nebular mass, including rotating and expanding gas, is low, $< 0.1 M_{\odot}$, often $\sim 0.01 M_{\odot}$ (Bujarrabal et al. 2013a). This suggests that they are not ejecting sufficient mass to form a high-mass PN (i.e., a nebula containing most initial mass). However, we point out that in many well-known PNe and pPNe the total detected nebular mass is smaller than $\sim 0.1~M_{\odot}$, including ionized gas, molecular gas, or PDR-like components; see, e.g., the compilation of mass values by Pottasch (1984), Huggins & Healey (1989), Huggins et al. (1996), Sánchez-Contreras et al. (2012), and Castro-Carrizo et al. (2001). It is also probable that the interaction of the star with the orbiting disk, including reaccretion of material, slows down their post-AGB evolution (e.g., Van Winckel et al. 2009). Indeed, all these NIR-excess stars still show relatively low stellar temperatures and exhibit spectral types usually in the range F-K. It is obvious that the conspicuous nebulae detected in some of these objects could form a low-mass PN, but the star would not necessarily become hot enough to ionize the surrounding gas before, due to expansion, the nebula becomes too diffuse to be detectable.

Most remarkably, disks are observed in binary post-AGB stars, which often show orbits that are too small to accommodate an AGB star (Van Winckel et al. 2009, Manick et al., 2017). In the best-studied NIR-excess post-AGB star, the Red Rectangle (Bujarrabal et al. 2016), the total angular momentum of the disk is not negligible in comparison to that of the binary at present. If, as expected, the disk angular momentum originates from the stellar system during a previous phase of strong interaction, a comparison of both the disk and binary momentum values at present implies that a significant decrease of the distance between the stars occurs (by a factor $\gtrsim 2$) from disk formation. We reach a similar conclusion from our observations; see detailed discussion in Sect. 4. These results suggest that the binary orbit was wider than the size of an AGB star in the past; but not much wider, which helps to explain the transfer of angular momentum. A better knowledge of the main properties of the disks is therefore imperative to understand the orbits of evolved binary stellar systems.

Finally, we recall that our post-AGB stars are not the only evolved stars surrounded by Keplerian disks. The existence of disks orbiting white dwarfs (WDs) has been known for more than three decades (e.g., Zuckerman & Becklin 1987, Bilíková et al. 2012). Some of these stars are also surrounded by prominent PNe, which are much more extended than the disks. It has been argued, see Clayton et al. (2014), that the Keplerian disks found in PNe are remnants of disks formed from circumstellar material ejected by the star in AGB or early post-AGB phases; this process is very similar to that probably responsible for the disks we are studying. The disks around very old WDs can be different; these disks possibly originate from the disruption of asteroids or analogs. Moreover, the presence of Keplerian rotation in a certain class of AGB stars, that is, semiregular variables that show aspherical shells in anisotropic slow expansion, has been also proposed. A relatively small disk has been well identified in one of these objects, L2 Pup (Homan et al. 2017). Our sources could therefore represent an evolutionary link between disks around AGB stars and disks around WDs (at least those surrounded by PNe), through the phase of prominent post-AGB disks. If this relation really holds, the disks surrounding WDs, whose mass is very low, would just contain a small fraction of the previous post-AGB disks, after a long process of disk evaporation.

We think that the study of disks orbiting NIR-excess post-AGB stars may be fundamental to the understanding of the formation of disks in various phases of the late evolution of intermediate-mass binary stars. This phenomenon can be crucial to understanding the late evolution of binary systems and the shaping of PNe.

We present ALMA maps of IRAS 08544–4431 in CO emission that clearly show both rotating and expanding gas. IRAS 08544–4431 is a low-amplitude pulsator that belongs to the class of NIR-excess post-AGB stars mentioned before (Maas et al. 2003, De Ruyter et al. 2006, Bujarrabal et al. 2013a, Hillen et al. 2016). The hot-dust component of IRAS 08544–4431 has been observed in the IR using the VLTI. The inner rim of the disk was imaged, showing a diameter of about 15 mas and suggesting an inclination with respect to the plane of the sky of about 20°. Our CO data confirm the disk-like structure and the value of the inclination, although the size of the CO-emitting region is much larger. IRAS 08544–4431 is a double stellar system; see Van Winckel et al. (2009). Assuming that the inclination of the orbit is that of the disk and a high-luminosity post-AGB primary

with $\sim 0.5~M_{\odot}$ at present, one deduces a $\sim 1-2$ -AU-wide orbit and a secondary with about 1.3 M_{\odot} ; but we stress that the mass of the individual stars is not well determined and strongly depends on the orbit inclination (see further discussion in Sect. 3.1).

These authors suggested a distance $D \sim 550$ pc for IRAS 08544–4431. However, this value is based on an assumed standard luminosity of 3000 L_{\odot} and is therefore very tentative. The GAIA parallax, 0.86 ± 0.6 mas, is not very accurate and we recall that the binary nature of the star can affect the parallax measurements in a complex way (Acke et al. 2013). As we see later in this work, $D \sim 1100$ pc is more compatible with our estimates of the total stellar mass, and we have adopted this value (see Sect. 3.1). We widely discuss the effects of the distance uncertainty on our modeling, in particular, to allow a comparison with previous results.

2. Observations

We present maps of IRAS 08544–4431 in the 12 CO and 13 CO J=3–2 lines, λ = 0.8 mm that were obtained with ALMA, band 7 receiver. A total of five observing runs were performed: three between August 29 and 30, 2015, and two more in August 25 and September 3, 2016. The source was observed for \sim 37 min in each track. The observations were obtained during ALMA Cycle 2. Thirty-four antennas were used with baselines ranging from 15 to 2483 m.

Data were calibrated with the CASA software package. The quasars J0538-4405, J0922-3959, and J0904-5735 were observed for bandpass, flux, and phase calibrations. Through a comparison of their fluxes in the different runs, we obtained significant differences between 2015 and 2016 observations, which is not exceptional in measurements of quasar continuum flux. The fluxes of the calibrators were found to change, respectively, from 886/372/464 mJy in 2015 to 1356/332/766 mJy in 2016. The flux calibration was however very consistent between the observations performed in the same year. Finally, by looking at final source data, in particular by comparing the source continuum emission obtained from 2015 data and 2016 observations, the flux calibration was judged to be optimal and no additional flux rescaling was applied.

After the data calibration, the rest of the analysis was made with the GILDAS software package. First, additional phase self-calibration was performed using the compact continuum source as reference. Image deconvolution was carried out with natural and also robust weighting, which leads to channel maps with 0.19×0.18 arcsec and 0.13×0.10 arcsec (HPBW) resolutions, respectively. Various CLEANing methods (Hogbom and SDI) were also used in the image synthesis to best represent the different emission components. The SDI method is known to be more adapted to represent the most extended emission. The data here presented were obtained with natural weighting and SDI method.

The ALMA backend was set to achieve a spectral resolution of about $0.2~{\rm km\,s^{-1}}$; the data were delivered with a channel spacing of $0.11~{\rm km\,s^{-1}}$). In the data presentation selected for this paper, the resolution was degraded to about $0.43~{\rm km\,s^{-1}}$ to improve the S/N at high velocities. We kept however the highest spectral resolution for the position-velocity diagrams to give a better representation of the velocity structure of the intense Keplerian disk. All velocity values in this paper are given in the Local Standard of Rest (*LSR*) frame.

By comparing our data with APEX single-dish profiles (Bujarrabal et al. 2013a), we conclude that a small fraction of

the flux, < 20%, was filtered out in the maps of 12 CO J=3–2. Anyway, we note that such moderate difference is close to usual uncertainties in absolute flux calibration. In addition, both single-dish and integrated ALMA profile shapes are very similar, confirming a low degree of lost flux. The 13 CO maps, with a less extended brightness distribution, are not expected to show a significant flux loss.

Dust continuum emission was found to be not resolved and centered at RA 08:56:14.165 DEC -44:43:10.588, which is also the center of all the maps here presented. Fitting of the continuum data in the uv-plane yielded a total flux of $\sim 320 \pm 1$ mJy and an estimated size of the emission region smaller than 0.1 arcsec. Such a continuum level was subtracted from our maps to better show the weakest features, in particular in the ^{13}CO position-velocity diagrams.

3. Modeling of our ALMA maps

The amount of data available for IRAS 08544–4431 and their quality are moderate, and these data are not comparable to those obtained for the best-studied NIR-excess post-AGB object, the Red Rectangle. We also lack information on the nebula in general. Under these conditions, very detailed models, such as those developed for the Red Rectangle, are not sensible and the uncertainties for several derived parameters are not negligible, as discussed below. Fortunately, the observational results in IRAS 08544–4431 are not very different from those obtained for the Red Rectangle, AC Her, 89 Her, and IW Car (Bujarrabal et al. 2007, 2015, 2016, 2017). In view of this, our models for IRAS 08544–4431 follow the general patterns found for these objects.

We used codes that are very similar to those described in our previous works (Bujarrabal et al. 2013b, 2015, 2017, ...). As for similar objects, all information we have on this nebula is compatible with the presence of axial symmetry. We assume local-thermal-equilibrium (LTE) populations for the involved rotational levels. This is a reasonable assumption for low-J CO transitions in the dense material expected in our sources, $n \gtrsim 10^4$ cm⁻³, since their Einstein coefficients are then smaller than the typical collisional rates; see further discussions in Bujarrabal & Alcolea (2013), Bujarrabal et al. (2016). The use of LTE may introduce some uncertainties (see below), but it significantly simplifies the calculations and provides an easier interpretation of the fitting parameters. For each considered model nebula, we assume a shape for the nebula, constant molecular abundances, and distributions of the local velocity dispersion, macroscopic velocity, density, and temperature. With these ingredients it is possible to calculate the absorption and emission coefficients of the two observed lines. These are computed for a high number of projected velocities, according to the actually observed channels, and for a high number of elemental cells occupying the whole nebula, typically around 10⁶ cells are used in our calculations. The cell density in general oversamples the central regions of the nebula, where the rotation velocity varies faster. We then solved the standard radiative transfer equation in a high number of directions pointing to the telescope (and for the set of projected velocities), taking into account the assumed orientation of the nebula axis with respect to the plane of the sky and to the north. Typically, we solve the transfer equations following 10⁴ to 10⁵ rays, which traverse the cells in which the nebula has been divided. We get a predicted brightness distribution, as a function of the coordinates (right ascension and declination offsets) and of the projected velocity. This distribution is numerically convolved with the interferometric clean beam and converted

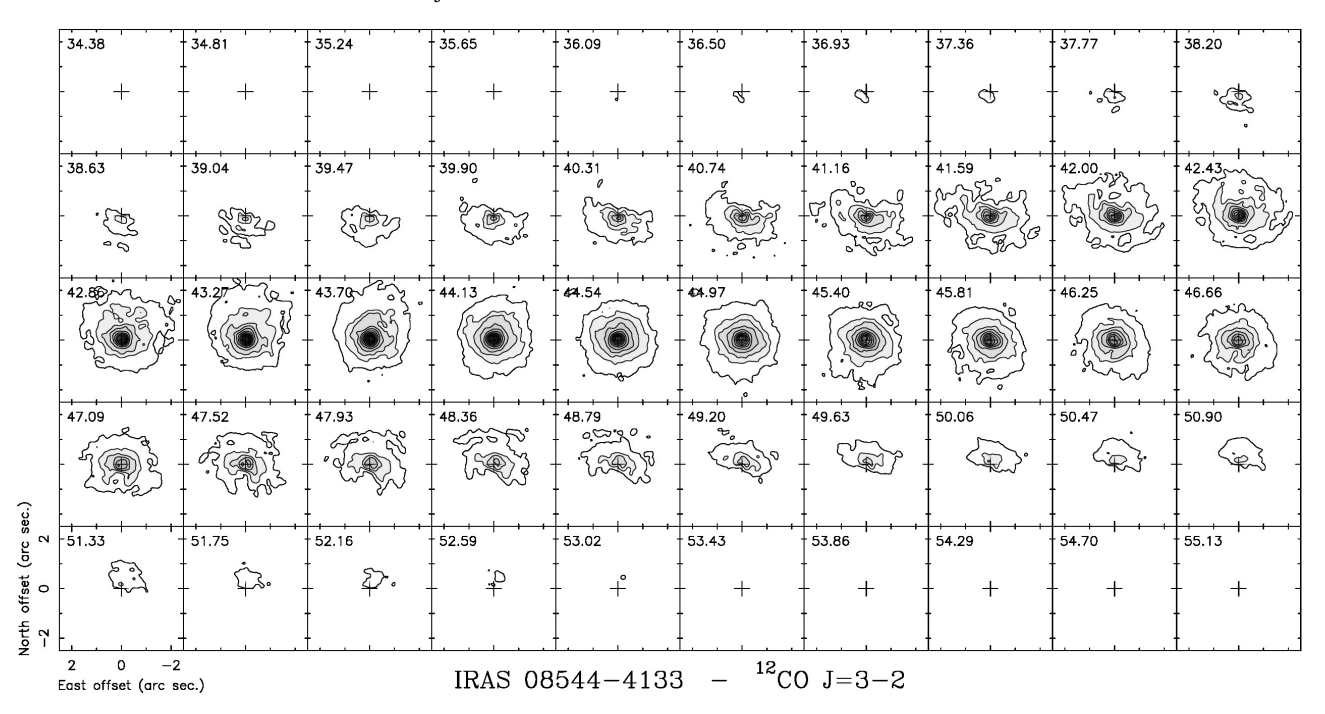


Fig. 1. ALMA maps per velocity channel of 12 CO J=3–2 emission in IRAS 08544–4431. The continuum emission has been subtracted to better show the distribution of the weak line. The first contour and spacing are 0.02 Jy beam⁻¹ (equivalent to 6 K, Rayleigh-Jeans equivalent temperature). The *LSR* velocities are indicated in each panel (upper left corner).

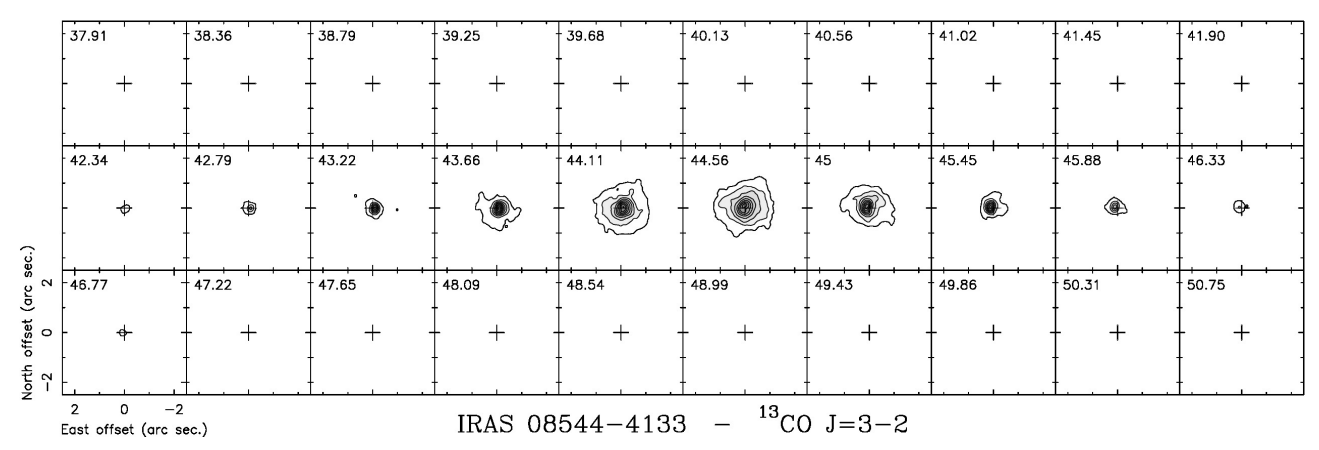


Fig. 2. ALMA maps per velocity channel of 13 CO J=3–2 emission in IRAS 08544–4431. The continuum has been also subtracted in this figure. The contours are shown as in Fig. 1: 0.02, 0.04, ... Jy beam⁻¹. The *LSR* velocities are indicated in each panel.

to units that are directly comparable to the observational data, Rayleigh-Jeans-equivalent brightness temperatures, or Jy/beam.

As mentioned, we took into account our results for better studied sources to select possible nebula models. In any case, a high number of different configurations were analyzed.

3.1. Description of the best-fit model

We finally adopted a model nebula as a good representation of the source, based on its reasonable properties and comparing the predictions with the observational data and other previous results; see predicted maps per velocity channel and position-velocity diagram in Figs. 3 and 5. Graphical representations of the main model parameters are given in Figs. 6 and 7. The parameters describing the best-fit model nebula, including those describing the main physical conditions, are given in Table 1. In principle, we give our results for an assumed distance D = 1100 pc. We have seen in Sect. 1 that the distance could be signifi-

cantly lower; the effects of the assumed distance on the derived parameters are discussed in Sect. 3.2, in which we consider in particular the case of an alternative distance of 550 pc.

In this best-fit model, we adopted a relative abundance with respect to the total number of particles $X(^{13}\text{CO}) \sim 1.5\ 10^{-5}$; as in most nebulae around evolved stars, we can assume that the dominant component of the low-excitation gas is H₂. This value of $X(^{13}\text{CO})$ is similar to those adopted in our previous works to ease the comparison with previous results on this and similar objects. Also following those works, we adopted an abundance ratio $^{12}\text{CO}/^{13}\text{CO} = 10$. Those values lead to a reasonable fit of the data.

The disk is assumed to be formed of two components. In the inner component, the rotation is purely Keplerian. The deduced velocity field corresponds to a central (stellar) mass of about 1.8 M_{\odot} , reasonable for this binary system (Sect. 1). In the outer component, we assumed sub-Keplerian rotation and the presence of a slow radial expansion, which significantly helps

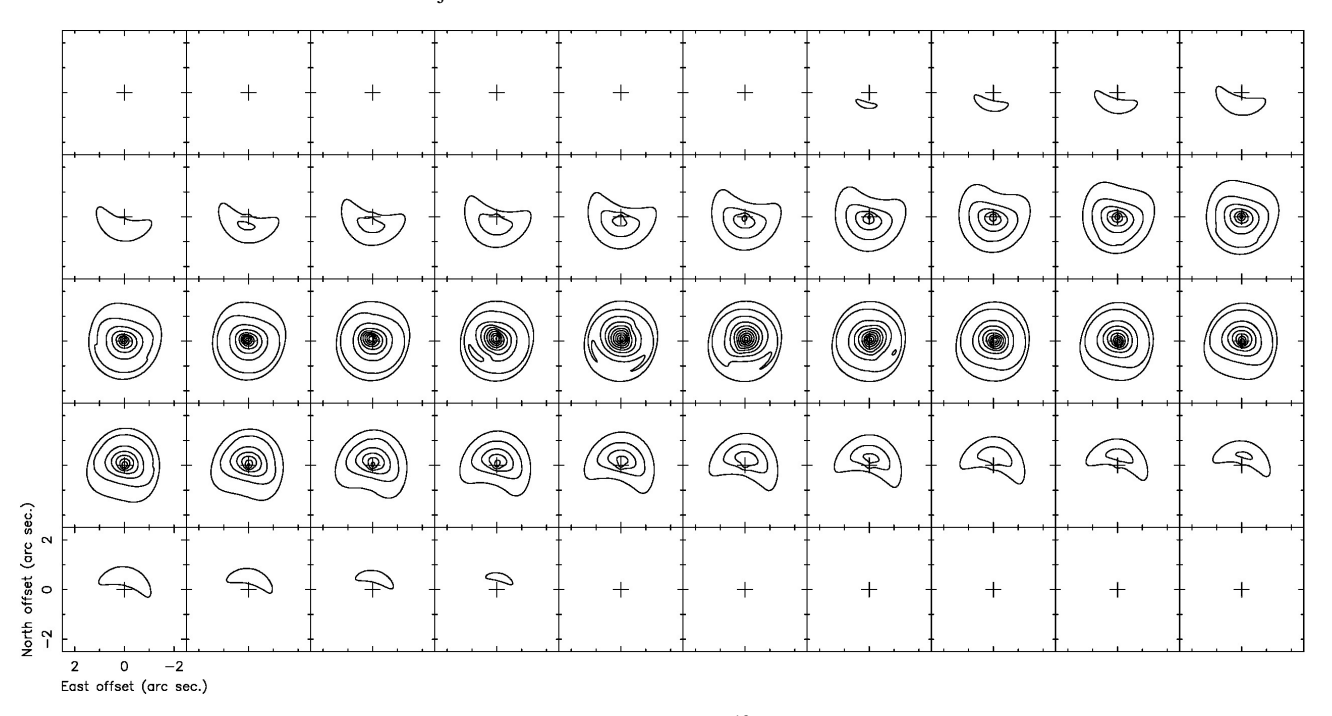


Fig. 3. Synthetic maps per velocity channel from our best-fit model of 12 CO J=3–2 emission in IRAS 08544–4431. These maps are comparable with Fig. 1; all scales and contours are the same as in that figure.

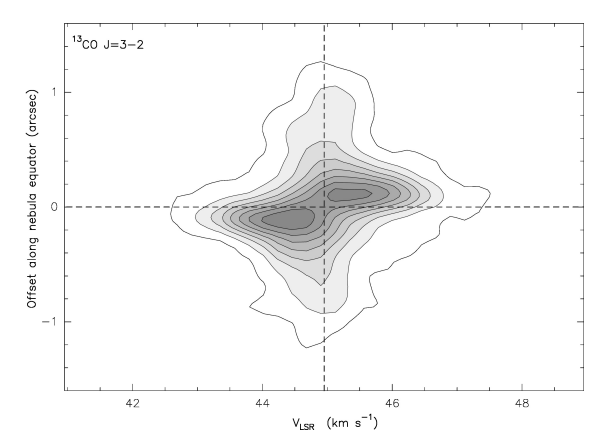


Fig. 4. Position-velocity diagrams from our ALMA maps of 13 CO J=3–2 in IRAS 08544–4431 along the direction P.A. = 75°. Contours are the same as in the channel maps, but we used a higher spectral resolution to better show the velocity structure. The dashed lines show approximate centroids in velocity and position

to reproduce the data, as was also the case in our studies of the Red Rectangle and IW Car (see discussions in our previous works, Bujarrabal et al. 2005, 2013b, 2017). For the sub-Keplerian velocity law we assumed angular momentum conservation. Remarkably, a similar result was independently found for L_2 Pup, the only AGB source in which a rotating disk has been found to date, by Homan et al. (2017), who also deduced sub-Keplerian rotation in the outer disk regions; in any case, the size of the disk around L_2 Pup is much smaller than in our objects.

We found that a small inner region of the disk must be devoid of molecules in some way. It is necessary to adopt an assumption of this kind to fit the high-velocity maps, but the angular resolution of our data does not allow a proper description of this region (see Sect. 3.2). A similar result was also found in our previous works for the Red Rectangle and IW Car. As in those papers,

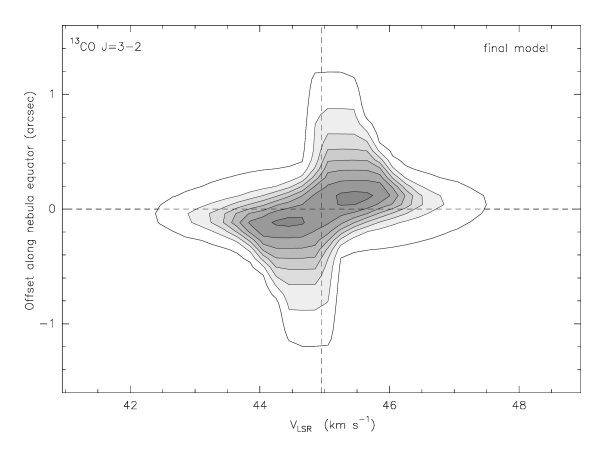


Fig. 5. Synthetic position-velocity diagrams from our best-fit model of 13 CO J=3–2 emission in IRAS 08544–4431, to be compared with Fig. 4; all scales and contours are the same as in that figure.

we assumed a progressive decrease of the disk width in the inner regions, instead of a sudden disappearance of the emitting gas. We recall that we cannot distinguish from fitting the different options, and here we take a simple law. An empty region at a smaller scale is also found in the IR VLTI maps of hot dust emission in IRAS 08544–4431 (Hillen et al. 2016), which show emission from a ring with a diameter of about 15 mas $(1-2\ 10^{14}$ cm, compatible with the dust sublimation radius). Those observations strongly select hot-dust inner regions and are probably able to trace the very inner disk, at the vertex of the cone depicted in Figs. 6 and 7, where the emission of the hottest dust is prominent despite its small radius and width.

In the disk, the density and temperature (n and T) are assumed to vary solely with the distance to the axis p and following potential laws; see values of the parameters in Table 1. We note the laws are not the same for both inner and outer disk

Table 1. Physical conditions in the molecule-rich nebula, derived from our model fitting of the CO data, and assuming D = 1100 pc. The values of the physical conditions depend on three geometrical parameters: the distance to the center, r, distance to the axis, p, and distance to the equator, h. See Figs. 6, 7 for more details and cartoons of the density, velocity, and temperature distributions.

		Inner disk Outer disk (pure Keplerian rotation) (subkeplerian rotation plus slow expansion)		Outflow		
Parameter	Law	Values	Law	Values	Law	Values
Radius (see Figs. 6, 7)	r < R _i	$R_i = 6 \ 10^{15} \ \text{cm}$	$r < R_o$	$R_o = 2 \ 10^{16} \ \text{cm}$	$p < R_{of}$	$R_{of} = 2.5 \ 10^{16} \ \text{cm}$
Total width (see Figs. 6, 7)	$h < H_i$	$H_i = 2.8 \ 10^{15} \ \text{cm}$	$h < H_o$	$H_o = 4 \ 10^{15} \ \text{cm}$	$h < H_{of}$	$H_{of} = 3.4 \ 10^{16} \ \text{cm}$
Temperature	$T = T_o \left(\frac{5 \cdot 10^{15} \text{cm}}{p}\right)^{\alpha_T}$	$T_o = 36 \text{ K}$ $\alpha_T = 0.4$	$T = T_o \left(\frac{10^{16} \text{cm}}{p} \right)^{\alpha T}$	$T_o = 27 \text{ K}$ $\alpha_T = 1$	$T = T_o \left(\frac{10^{16} \text{cm}}{r} \right)^{\alpha_T}$	$T_o = 50 \text{ K}$ $\alpha_T = 0.7$
Density	$n = n_o \left(\frac{5 \cdot 10^{15} \text{cm}}{p}\right)^{\alpha_n}$	$n_o = 3.7 \ 10^6 \ \text{cm}^{-3}$ $\alpha_n = 1$	$n = n_o \left(\frac{10^{16} \text{cm}}{p}\right)^{\alpha_n}$	$n(10^{16} \text{cm}) = 9 \cdot 10^5 \text{ cm}^{-3}$ $\alpha_n = 1$	$n = n_o \left(\frac{10^{16} \text{cm}}{r}\right)^{\alpha_n}$	$n_o = 8.5 \ 10^4 \ \text{cm}^{-3}$ $\alpha_n = 2.3$
Local velocity dispersion	constant	$0.1 \; {\rm km \; s^{-1}}$	constant	$0.1 \; {\rm km s^{-1}}$	constant	$2\;\mathrm{km}\mathrm{s}^{-1}$

Other parameters	Law	Values	comments
Axis inclination with respect to the plane of the sky		70°	from IR and CO data
Axis inclination in the plane of the sky (PA)		-15°	from IR and CO data
Distance		1100 pc	various arguments (Sect. 1)
¹² CO relative abundance ¹³ CO relative abundance	constant constant	1.5 10 ⁻⁴ 1.5 10 ⁻⁵	this paper this paper

components. The density distribution is shown in Fig. 6. As in our previous works, we find that the disk must show a very small local velocity dispersion to fit the data; we assumed that this is the combination of the thermal movements and a small local dispersion (microturbulence) of 0.1 km s^{-1} .

In the outflow, the density and temperature are assumed to vary with the distance to the center, again following potential laws; see parameters in Table 1. The expansion velocity is basically radial and has a minor component that is parallel to the equator. The local velocity dispersion in the outflow is dominated by microturbulence with a dispersion of 2 km s⁻¹.

The total nebular mass derived from our fitting is $\sim 2\ 10^{-2}\ M_{\odot}$, about 90% of which is placed in the disk. These values are compatible with those found by Bujarrabal et al. (2013a, after correcting the different assumed distance), although their treatment, based only on single-dish ¹²CO observations, was much more uncertain. From the extent and velocity field of the expanding envelope, we derived a typical time required to form it of about 1100 yr. From the disk/outflow mass ratio and assuming, as we deduced for similar sources (Sect. 1), that the outflowing gas has been expelled from the disk, we can estimate a disk lifetime of about 10000 yr. This value is comparable to that found for IW Car and the Red Rectangle. This is just an estimate of the disk lifetime scales, since the mass-ejection rate can vary with

time. We also stress that our outflow component is unbounded, since the escape velocity is $\sim 1.8~\rm km\,s^{-1}$ at 1000 AU, a few times smaller than the outflow velocity.

As we discuss in Sect. 3.2, the derived parameters are affected by the adopted distance, whose value is not well known (Sect. 1). If we assume a significantly shorter distance, as mentioned in the Introduction, ~ 550 pc, most model parameters change significantly and IRAS 08544-4431 becomes a relatively small and low-mass post-AGB nebula. The total size would be $\sim 3.5 \cdot 10^{16}$ cm (lower than for the Red Rectangle) and the total mass would become $\sim 6 \cdot 10^{-3} M_{\odot}$ (the mass of the Red Rectangle is $\sim 10^{-2} M_{\odot}$). The central stellar mass and the disk lifetime would become $\sim 0.9~M_{\odot}$ and $\sim 5000~\rm{yr}$, again lower than those of the Red Rectangle. In view of the parameters deduced for the stellar orbit, Sect. 1, a total mass of about 1.8 M_{\odot} would be necessary to get a mass of the primary of about 0.5 M_{\odot} , a very reasonable value for a post-AGB star. A total mass of $\sim 1 M_{\odot}$, as deduced for 550 pc, would yield a primary mass of only 0.1 M_{\odot} . Therefore, this reasoning favors a long distance ~ 1100 pc for IRAS 08544–4431, which is taken as our standard value, but its validity depends on the relatively uncertain mass

A distance of 1.1 kpc implies a luminosity $\sim 12000~L_{\odot}$. Using the core-mass luminosity relation of Miller Bertolami

(2016), this results in a post-AGB mass of about 0.65 M_{\odot}. But a larger primary mass requires a larger total mass (as deduced from the orbit mass function and inclination), and then still larger distance (to explain the observed disk rotation) and luminosity. To be fully compatible with the stellar evolution calculations, we should adopt a distance ~ 1.5 kpc, a primary mass ~ 0.8 M_{\odot} , a total mass of 2.5 M_{\odot} , and a luminosity of about 2 10⁴ L_{\odot} . However, this criterion is weak because of the poorly understood post-AGB evolution of the stars studied here (Sect. 1) and the difficulties in measuring the involved parameters, widely mentioned in this paper. In particular, total stellar mass values of $2-2.5~M_{\odot}$ are still compatible with a distance of 1.1 kpc and the observed Keplerian velocity field (within the uncertainties, Sect. 3.2). The orbital parameters are also uncertain; in particular, the translation from observed orbital parameters to physical binary parameters is strongly dependent on the inclination. An orbital inclination of 23°, a change of just 3° with respect to our standard value, and a post-AGB mass of 0.65 M_{\odot} give a total stellar mass of 1.8 M_{\odot} from the measured mass function. This is compatible with the gravitational mass obtained from the ALMA data and with evolution calculations for our distance value, 1.1 kpc. Moreover, a significantly larger distance would lead to very high values of the nebular mass and size compared with results for other similar objects (Sect. 1). Accordingly, we think that the distance derived from the parallax measurements, 1.1 kpc, is a reasonable compromise that is compatible with all the available information.

We derived the disk angular momentum by integrating the local momentum of the volume units for the adopted density and velocity laws. The uncertainties of this estimate are discussed in Sect. 3.2. Particularly interesting is the distance dependence of the disk angular momentum. For a distance of 550 pc, we derived a disk angular momentum $J \sim 1.6~M_{\odot}~{\rm km}~{\rm s}^{-1}$ AU. This value is significantly smaller than that of the Red Rectangle ($\sim 9~M_{\odot}~{\rm km}~{\rm s}^{-1}$ AU), but still high for the low central mass deduced in that case. The strong dependence $J \propto D^3$ (Sect. 3.2) yields a high value $J \sim 13~M_{\odot}~{\rm km}~{\rm s}^{-1}$ AU for our best distance estimate, $D = 1100~{\rm pc}$. The angular momentum of the stellar system at present is found to be $\sim 20~M_{\odot}~{\rm km}~{\rm s}^{-1}$ AU, comparable to that of the disk. The stellar parameters used for this estimate are given in Sect. 1; see more details and discussion in Van Winckel et al. (2009). Again an angle between the orbit and sky planes of about 20° is assumed.

3.2. Uncertainties in the derivation of the model parameters

Some disk properties are not well determined from the observations, mainly because of the relatively low angular resolution and the weak dependence of the predictions on these properties. In particular, the width of the disk is not well determined because of the insufficient angular resolution and significant inclination of the axis with respect to the plane of the sky. The size and shape of the central region of the disk is assumed to show a decreasing width, which is a result similar to that we found in previously studied nebulae. The exact shape of these regions is also difficult to measure, in fact, we take a typical diameter of 2 10¹⁵ cm (for D = 1100 pc) that is smaller than the resolution in linear units, 3 1015 cm. An inner disk region with relatively low CO emission clearly improves the quality of the modeling and is in fact necessary to get a reasonable data fitting, but we must keep in mind the uncertain structure of these very inner disk regions. On the contrary, the diameter of the disk is well measured, since it is basically given by its extent in the maps, that is, much larger than the resolution.

The general structure of the wide outflow is also well determined from the data. However, the details of the boundary shape are of course uncertain, mainly in the farther regions of the X-shaped structure, whose emission is weak. Because of the relatively large total extent, comparable to the distance at which CO is photodissociated by the interstellar UV field in expanding gas, it is probable that the actual shape of the emitting region is rather due to CO photodissociation than to a relatively sudden decrease of the density; for the relatively low mass-loss rates characteristic of the outflows in our sources, see Mamon et al. (1988), Groenewegen (2017). Any attempt to deduce the size and shape of the CO-rich gas from the dissociation theory is extremely difficult because of the uncertainties in the path covered by each gas particle and the unknown changes of the velocity with time. We think that the general nebula shape we propose in this paper, after incorporating our previous experience with similar sources, is realistic and could be transferred, with moderate scaling and changes, to most of the sources of this kind.

The total mass of both nebular components is relatively well constrained (for an assumed distance) because we match the total intensity of optically thin emission: ¹³CO emission for the disk and inner outflow regions and ¹²CO emission for the outermost regions. The main source of uncertainty for the total mass comes from the assumed value of the CO abundances, $X(^{12}CO,$ ¹³CO). Because of the LTE approach we used, there is a degeneracy between density and CO abundance, such that predictions are identical for values of both parameters keeping a constant product. The errors in the mass are, therefore, inversely proportional to those of the abundance. Fortunately, these abundances are not very uncertain, showing a moderate variation between different studies. Following discussions in our previous works, we estimate $X(^{13}CO)$ and $X(^{12}CO)$ must vary in the ranges 10^{-5} $-2 \cdot 10^{-5}$ and $10^{-4} - 2 \cdot 10^{-4}$, respectively. We so expect a moderate uncertainty in the estimate of the molecule-rich gas mass, $\sim \pm 50\%$. The degree of uncertainty in the estimate of the disk angular momentum is similar to that of the total mass (or just slightly larger), since the detected disk radius and velocity are relatively well measured. We cannot rule out the presence of outer regions that may remain undetected because of their low brightness or photodissociation. Therefore, the derived mass and momentum values may be lower limits corresponding to the actually detected gas.

The values of the temperature are relatively uncertain because we only have data of J=3–2 emission. However, we note the high brightness of optically thick emission (12 CO line) from the disk and inner outflow, > 30 K, reaching values close to 100 K. These are comparable to the high brightness found in the Red Rectangle, AC Her, and IW Car, suggesting high temperatures similar to those we deduced in our previous papers, over 100 K in central regions and decaying outward. Further details on the temperature distribution are difficult to estimate.

The uncertainty in the average gas density in the disk can be important, mainly because of the uncertain disk width, with variations of the density inversely proportional to those of the width. The value adopted for X also affects the values deduced for the density, as mentioned above. The density is particularly difficult to estimate in the outer regions of the outflow because of the low emission and more uncertain temperature law there. It is difficult to determine the effect that the temperature uncertainty has on the density estimate, but it is probably moderate. In principle, n is appoximately proportional to the assumed value of T for temperatures much higher than the line excitation (\sim 30 K), exact LTE, and very low opacities. But the dependence is signif-

icantly lower than linear and tends to vanish when the excitation temperature is not very high or the optical depth is moderate.

The derived disk/outflow mass ratio and disk lifetime bear somewhat stronger uncertainties than the independent mass values because a change in the abundances affects the determinations of the mass in both components in different ways. The uncertainty in the values of X(CO) mentioned above leads to changes in the disk lifetimes between 5000 and 2 10^4 yr.

The velocity fields, both rotation and expansion, are relatively well measured, since maps are obtained for well-known LSR velocities and the nebula inclination is well constrained. Of course, the exact direction of the velocity, i.e., the inclination of the arrows in Fig. 6, can significantly change. For instance, we cannot rule out a purely radial velocity (as found for IW Car). In any case, we had problems fitting the data with simple models that include radial velocities; the assumption of a radial velocity field would probably require small changes in the symmetry axis direction with the distance to the center. The central stellar mass depends on the square Keplerian velocity; therefore, even for small changes in the velocity of 15%, we can expect variations in the stellar mass of about 30%. The same applies for errors in the estimate of the inclination angle, since they affect the measurement of the Keplerian velocity modulus. We estimate that the stellar mass uncertainty is of about 40%.

The distance of the object D is very uncertain (Sect. 1), which affects the other parameters. The model nebula size must vary linearly with the distance to continue to fit the data. The velocity field is not affected, provided that we scale the velocity laws to the size of the nebula. The same rule holds for the temperature. The density varies with D^{-1} , after scaling the density law to the size of the nebula since the column density must be conserved to yield the same optical depth in all lines of sight. Therefore, the change in the total volume implies that the total mass varies with D^2 . The variations of the rotation velocities and distances mentioned above imply that the central stellar mass varies proportionally to the assumed distance. The dependencies of the velocity and size also lead to variations of the disk lifetime, proportionally to D. The dependence of the disk angular momentum on the distance is particularly strong, varying with the third power of the assumed value, since the momentum of an elementary particle rotating at a given velocity depends on its total mass and distance to the axis. These dependence laws are basically the same in all models of molecular line emission from AGB or post-AGB shells.

Finally, we note that some features of our observations are not well reproduced by our model. Most of them are minor details, and probably correspond to the actual complexity of the true nebula in comparison with our very simple model. The most important discrepancy, in our opinion, is the presence of a shift to relatively low LSR velocities of the central maximum in the ¹²CO maps. This would correspond to an asymmetry in the emission between the gas that rotates approaching us, which is brighter, and that receding from us. Since the effect is less noticeable in ¹³CO maps, the natural explanation is that the kinetic temperature is higher in the disk edges at certain azimuthal angles. We can speculate that the position of the central stars can lead to a selective heating of certain regions of the disk. We do not try to incorporate these phenomena in our nebula model, since their nature is very uncertain and other complex effects could be present, such as selective photodissociation and gas evaporation. The effects of such a selective heating on the derived physical parameters remains within the ranges discussed before.

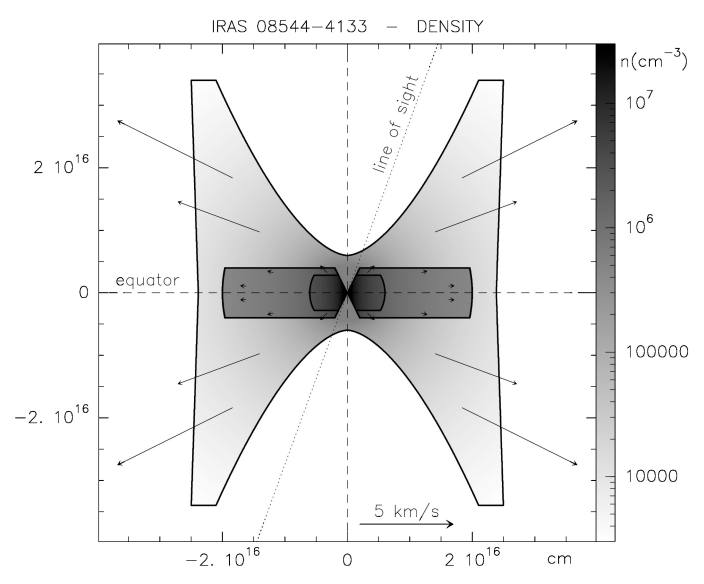


Fig. 6. Density and velocity distributions in our best-fit model. The model is shown for D = 1100 pc; the length scale would change proportionally for other distance values. Only expansion velocities are shown because we represent a plane containing the symmetry axis; rotation is only present in the equatorial disk.

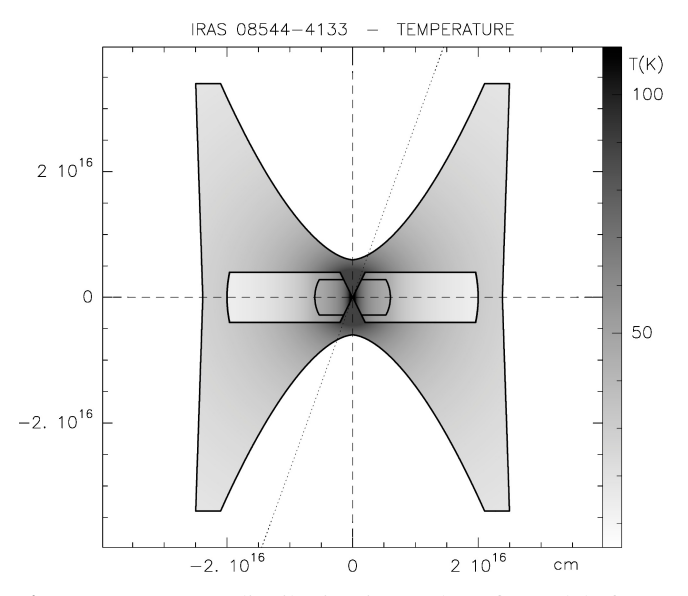


Fig. 7. Temperature distribution in our best-fit model (for D = 1100 pc).

4. Conclusions

We present high-quality ALMA maps of 12 CO and 13 CO J=3–2 emission from IRAS 08544–4431 (Sect. 2) and detailed modeling able to explain the main observational features (Sect. 3). IRAS 08544–4431 belongs to a class of binary post-AGB stars that are known to show indications of being surrounded by material in rotation (Sect. 1), including a significant NIR excess (supposed to be due to emission of hot dust) and peculiar CO line profiles that are very similar to those expected from rotating disks. The presence of rotating disks was previously confirmed by maps of the velocity field in three of these sources, the Red Rectangle, IW Car, and AC Her. A component of gas in expansion, probably expelled from the disk, is also confirmed in five and probably present in most of these objects (Sect. 1). Both rotating and outflowing components were only well detected in the

Red Rectangle and IW Car. Our maps of IRAS 08544-4431 also show a clearly composite nebula with a disk in rotation and gas in expansion. The general properties of our maps and modeling of IRAS 08544-4431 are remarkably similar to those found in better studied similar objects, such as the Red Rectangle, which confirms our interpretation.

We analyze the CO emission by means of nebula models accounting for the complex nature of the source. From our model fitting, we derive the main nebula parameters: shape and velocity field, density distribution and total mass, and characteristic temperature (Sect. 3). We extensively discuss the uncertainties in the derivation of those parameters in Sect. 3.2, in particular the dependence of the derived properties on the distance of the star. We adopt a distance D = 1100 pc, but we are aware of that this value is uncertain and also discuss the case of a distance smaller by a factor 2 (Sect. 1), particularly to compare our conclusions with previous results. The mass of the nebula is found to be ~ $2 \cdot 10^{-2} M_{\odot}$ (~ $6 \cdot 10^{-3} M_{\odot}$ for D = 550 pc), and about 90% of the nebular material would be placed in the disk. These values are compatible with those typically found in similar sources, as well as with previous estimates for IRAS 08544-4431 from much less complete data (Bujarrabal et al. 2013a). The mass of the central stellar system is derived from analysis of the rotation dynamics. We find a central mass of about 1.8 M_{\odot} (0.9 M_{\odot}). The higher stellar mass value is comparable to the result found for the Red Rectangle, while $0.9 M_{\odot}$ is very similar to that of the IW Car. A high stellar mass value is more compatible with the measured properties of the binary system, which is composed of a very luminous post-AGB primary with roughly $0.5 - 0.8 M_{\odot}$ and a more massive secondary (see Sects. 1, 3.1). In spite of the uncertainties, the need for a relatively high total mass favors a distance of about 1100 pc for IRAS 08544-4431. The typical size of the nebula is $\sim 6 \cdot 10^{16}$ cm ($\sim 3 \cdot 10^{16}$ cm for D = 550 pc). As for other well-studied objects, only the central part of the disk is in purely Keplerian rotation; the rotation of the outer disk is probably sub-Keplerian and a slow expansion appears in it. A similar result was found in the Red Rectangle and IW Car, and in the only AGB star in which a rotating disk has been found, i.e., L₂ Pup (Homan et al. 2017)

It is remarkable that, for the low distance value we considered, i.e., D = 550 pc, the nebula would show relatively low mass and size and the total stellar mass would be relatively low compared to those of the Red Rectangle (the best studied object of this class), but closer to the properties of IW Car. However, for our best distance value, $D \sim 1.1$ kpc, IRAS 08544-4431 is slightly larger and more massive than the Red Rectangle. We propose that the Red Rectangle and IRAS 08544-4431 are relatively similar objects.

The angular momentum found in the disk (for D = 1.1 kpc) reaches a high value $J \sim 13 M_{\odot} \,\mathrm{km \, s^{-1}}$ AU, which is comparable to that found for the binary system at present ($\sim 20~M_{\odot}~{\rm km\,s^{-1}}$ AU, see Sects. 3.1 and 1). In our case, it is expected that the disk angular momentum comes from the binary system because the gas is ejected with negligible rotation. Therefore, and keeping in mind the uncertainties that affect these measurements, we deduce that the binary angular momentum was $\sim 33~M_{\odot}~{\rm km\,s^{-1}}$ AU in the past. Since in a binary star J is basically proportional to the square root of the orbit size, we conclude that the distance between the stars has significantly decreased, by a factor $\gtrsim 2$, owing to the transfer of angular momentum to form the disk. The orbit was probably larger than an AGB star, but not much larger, which allowed a significant momentum transfer. The moderate orbit size change indicates that the system certainly had momentum enough to explain the disk rotation, while maintaining a size of some astronomical units during the whole process. We hope that these results serve to better understand the evolution of binary stars in the presence of dense circumstellar material and as a comparison with theoretical studies of the transfer of angular momentum to circumbinary disks (Chen et al. 2017, Akashi & Soker 2008, Dosopoulou & Kalogera 2016, etc).

We conclude that these NIR-excess post-AGB objects systematically show composite nebula, which contain relatively extended disks in rotation, plus gas in slow expansion that is probably escaping from the disk. The total mass of such nebulae is small compared with those of most PNe and pPNe (Sect. 1), i.e., $< 10^{-1}~M_{\odot}$ and often $\sim 10^{-2}~M_{\odot}$. The mass of the outflow is several times lower than that of the disk in well-studied cases. IRAS 08544-4431 is the third object in which these nebular structure and dynamics are well established and the main properties of both components are described.

Acknowledgements. This work has been supported by the Spanish MINECO (grants AYA2012-32032, FIS2012-32096, and AYA2016-78994-P), and by the European Research Council (ERC Grant 610256: NANOCOSMOS). We used the SIMBAD database to check some properties of the source. We are grateful to the referee of this paper, Dr. O. de Marco, for her constructive comments. This paper makes use of the following ALMA data: ADS/JAO.ALMA#2013.1.00338.S. ALMA is a partnership of ESO (representing its member states), NSF (USA) and NINS (Japan), together with NRC (Canada), MOST and ASIAA (Taiwan), and KASI (Republic of Korea), in cooperation with the Republic of Chile. The Joint ALMA Observatory is operated by ESO, AUI/NRAO and NAOJ.

References

Acke, B., Degroote, P., Lombaert, R., et al. 2013, A&A, 551, A76 Akashi, M., & Soker, N. 2008, New A, 13, 157 Alcolea, J., Neri, R., & Bujarrabal, V. 2007, A&A, 468, L41 Balick, B., & Frank, A. 2002, ARA&A, 40, 439 Bilíková, J., Chu, Y.-H., Gruendl, R. A., Su, K. Y. L., & De Marco, O. 2012,

ApJS, 200, 3

Bujarrabal, V., Castro-Carrizo, A., Alcolea, J., & Sánchez Contreras, C. 2001, A&A, 377, 868

Bujarrabal, V., Castro-Carrizo, A., Alcolea, J., & Neri, R. 2005, A&A, 441, 1031 Bujarrabal, V., van Winckel, H., Neri, R., et al. 2007, A&A, 468, L45

Bujarrabal, V., & Alcolea, J., 2013, A&A, 552, A116

Bujarrabal, V., Alcolea, J., Van Winckel, H., Santander-García, M., & Castro-Carrizo, A. 2013a, A&A, 557, A104

Bujarrabal, V., Alcolea, J., Van Winckel, H., et al. 2013b, A&A, 557, L11 Bujarrabal, V., Castro-Carrizo, A., Alcolea, J., & Van Winckel, H. 2015, A&A,

Bujarrabal, V., Castro-Carrizo, A., Alcolea, J., et al. 2016, A&A, 593, A92 Bujarrabal, V., Castro-Carrizo, A., Alcolea, J., et al. 2017, A&A, 597, L5 Castro-Carrizo, A., Bujarrabal, V., Fong, D., et al. 2001, A&A, 367, 674 Castro-Carrizo, A., Neri, R., Bujarrabal, V., et al. 2012, A&A, 545, A1 Chen, Z., Frank, A., Blackman, E. G., Nordhaus, J., & Carroll-Nellenback, J. 2017, MNRAS, 468, 4465

Clayton, G. C., De Marco, O., Nordhaus, J., et al. 2014, AJ, 147, 142 De Marco, O. 2009, PASP, 121, 316

De Marco, O., Passy, J.-C., Moe, M., et al. 2011, MNRAS, 411, 2277 De Marco, O. 2014, Asymmetrical Planetary Nebulae VI Conference, 122

de Ruyter, S., van Winckel, H., Maas, T., et al. 2006, A&A, 448, 641 Dosopoulou, F., & Kalogera, V. 2016, ApJ, 825, 71

Gezer, I., Van Winckel, H., Bozkurt, Z., et al. 2015, MNRAS, 453, 133 Groenewegen, M. A. T. 2017, A&A, 606, A67

Hillen, M., Kluska, J., Le Bouquin, J.-B., et al. 2016, A&A, 588, L1 Hillen, M., Van Winckel, H., Menu, J., et al. 2017, A&A, 599, A41

Hillwig, T. C., Jones, D., De Marco, O., et al. 2016, ApJ, 832, 125 Homan, W., Richards, A., Decin, L., et al. 2017, A&A, 601, A5

Hrivnak, B. J., Van de Steene, G., Van Winckel, H., et al. 2017, ApJ, 846, 96 Huggins, P. J., & Healy, A. P. 1989, ApJ, 346, 201

Huggins, P. J., Bachiller, R., Cox, P., & Forveille, T. 1996, A&A, 315, 284 Iaconi, R., Reichardt, T., Staff, J., et al. 2017, MNRAS, 464, 4028

Maas, T., Van Winckel, H., Lloyd Evans, T., et al. 2003, A&A, 405, 271

Manick, R., Van Winckel, H., Kamath, D., Hillen, M., & Escorza, A. 2017, A&A, 597, A129

Miller Bertolami, M. M. 2016, A&A, 588, A25

Olofsson, H., Vlemmings, W. H. T., Maercker, M., et al. 2015, A&A, 576, L15

V. Bujarrabal et al.: ALMA observations of IRAS 08544-4431

Pottasch, S. R. 1984, "A study of late stages of stellar evolution", Astrophysics and Space Science Library, 107

Soker, N. 2001, ApJ, 558, 157

Sánchez Contreras, C., Sahai, R., & Gil de Paz, A. 2002, ApJ, 578, 269
Sánchez Contreras, C., Gil de Paz, A., & Sahai, R. 2004, ApJ, 616, 519
Sánchez Contreras, C., & Sahai, R. 2012, ApJS, 203, 16
Santander-García, M., Bujarrabal, V., Alcolea, J., et al. 2017, A&A, 597, A27

Van Winckel, H. 2003, ARAA, 41, 391

Van Winckel, H., Lloyd Evans, T., Briquet, M., et al. 2009, A&A, 505, 1221 Zuckerman, B., & Becklin, E. E. 1987, Nature, 330, 138